Deltares

Influence of railway track degradation on vibration generation



Influence of railway track degradation on vibration generation

Author(s)

dr. B. E. Zuada Coelho



Influence of railway track degradation on vibration generation

Client	ProRail				
Contact	de heer H. Zandberg				
Reference					
Keywords					
Document control					
Version	1.0				
Date	26-10-2023				
Project nr.	11207953-002				
Document ID	11207953-002-GEO-0004				
Pages	43				
Classification					
Status	final				
And and a					
Author(s)					
	Bruno Zuada Coelho				

The allowed use of this table is limited to check the correct order-performance by Deltares. Any other client-internal-use and any external distribution is not allowed.

Doc. version	Author	Reviewer	Approver
1.0	Bruno Zuada Coelho	Paul Holscher	Remon Pot

Summary

This report concerns the study of the effect of the railway track deformation on railway induced vibrations. The study focuses on the analysis of two railway track objects (transition zone and rail joint), and the resulting railway track deformation that takes placed given a realistic traffic scenario, during a period of one year. The analyses are performed for two different realistic subsoil conditions, based on two locations along the A2 corridor: stiff and soft subsoil. The results of the track deformation are used to compute ProRail's newly proposed railway track vibration quality parameters, H_{max} and H_{rms}.

Spatial variability emerged as a more significant factor than rail irregularities in addressing railway track deformation. Ballast compaction initially dominated track deformation, but over time, subsoil creep and consolidation took precedence.

Displacement was notably higher near transition zones compared to the free track further away, aligning with findings from existing literature. For rail joints, their influence was most prominent at high frequencies, which are less relevant to track deformation.

The parameters H_{max} and H_{rms} were observed to remain constant over different time periods for a given railway track object. However, the railway track deformation exhibited significant variation during these intervals. This suggests that the railway track deformation does not have an impact on the induced vibrations which is not in agreement with experimental evidence. It is important to note that this results to not negate the potential impact of railway track deformation on induced vibrations. Rather, it suggests that the parameters H_{max} and H_{rms} are not able to detect these effects. The parameters H_{max} and H_{rms} should be expanded to encompass lower and higher wavelengths, allowing for the consideration of spatial variability, railway irregularities, and discontinuities. This would enhance their effectiveness in capturing a broader range of effects.



Contents

	Summary	4
1	Introduction	7
2	Methodology	8
2.1	General description	8
2.2	Train-track dynamic analysis	8
2.3 2.3.1 2.3.2	Rail irregularities Vertical profile rail Rail joints	9 9 10
2.4	Subsoil dynamic stiffness and damping	10
2.5 2.5.1 2.5.2	Cumulative cyclic deformation Model ballast settlement Model subsoil settlement	11 12 14
2.6	Spatial variability	15
2.7	Track vibration quality parameters	15
3	Case study description	16
3.1 3.1.1 3.1.2	Analyses description Transition zone Rail joint	16 16 17
3.2 3.2.1 3.2.2	Subsoil description and characterisation Subsoil description Subsoil characterisation	17 17 18
3.3	Railway track	19
3.4	Ballast	20
3.5 3.5.1 3.5.2	Train loading scenarios Passenger trains Freight trains and locomotives	20 20 20
4	Results	23
4.1 4.1.1 4.1.1.1 4.1.1.2 4.1.1.3 4.1.2 4.1.2.1 4.1.2.2 4.1.2.3	Transition zone Soft to stiff subsoil Without irregularities Effect of irregularities Effect of spatial variability Stiff to soft subsoil Without irregularities Effect of irregularities Effect of spatial variability	23 23 23 24 25 26 26 26 27
4.2 4.2.1	Rail joint Soft subsoil	28 28



	Appendix A	42
6	References	39
5.2	Recommendations	38
5.1.2	Does a reduction in maintenance intervals at track objects result in a proportionally higher track vibration quality?	37
	How does the "track vibration quality" develop over time at track objects (crossing structures and ES-joints) given a train loading scenario?	37
5.1 5.1.1	Conclusions How does the "track vibration quality" develop over time at track chicate (crossing	37
5	Conclusions and recommendations	37
4.3.3	Discussion on parameters H _{max} and H _{RMS}	36
4.3.2.2	Stiff subsoil	35
4.3.2.1	Soft subsoil	35
4.3.2	Rail joint	35
4.3.1.2	Stiff to soft subsoil	34
4.3.1.1	Soft to stiff subsoil	33
4.3 4.3.1	H _{max} and H _{rms} Transition zone	აა 33
		33
4.2.2.2 4.2.2.3	Effect of irregularities Effect of spatial variability	32
4.2.2.1 4.2.2.2	Without irregularities Effect of irregularities	31 31
4.2.2	Stiff subsoil	31
4.2.1.3	Effect of spatial variability	30
4.2.1.2	Effect of irregularities	29
4.2.1.1	Without irregularities	28

1 Introduction

In the context of the Innovatieagenda Bronaanpak Spoortrillingen (IBS), ProRail has defined various projects for developing monitoring techniques for track vibrations. One of the projects is the investigation of the usefulness of the railway track geometry dataset presented in the Branche Breed Monitoring Systeem (BBMS) for assessing track quality in relation to vibration nuisance (in the Netherlands, track geometry is monitored using a Track Recording Car). ProRail has commissioned Level Acoustics & Vibration [1] to analyse historical track geometry data with the aim of defining parameters that describe track quality for vibration nuisance. The historical track geometry data is linked to data from track objects, such as railway crossings, electrical separation joints (rail joints), bridges, and underpasses.

The analysis based on PSD (Power Spectral Density) shows that the track quality in relation to vibration nuisance is log-normally distributed and that the largest vibrations are expected when a track object is presented. The research presented in [1] suggests that dynamic forces on the track structure are the largest at these locations, and the associated vibrations are higher compared to a continuous track structure. In [1] the track vibration quality is described with two parameters H_{max} and H_{rms} . However, based on the analysis of historical data, it is not well supported which target value should be used for the track vibration quality.

Because it is unclear which target value is realistic and which additional maintenance efforts are associated with it, it is necessary to investigate the relationship between the level of track vibration quality and the speed of track degradation at track objects given an annual train traffic load. Based on the preceding considerations, ProRail has defined the following research questions to Deltares:

- 1. How does the "track vibration quality" develop over time at track objects (transition zones and rail joints) given a train loading scenario?
- 2. Does a reduction in maintenance intervals at the track objects (transition zones and rail joints) result in a proportionally higher track vibration quality?



2 Methodology

2.1 General description

To model the railway track degradation that takes place in the vicinity of track objects, the following methodology is followed:

- 1. Generation of the input geometry (rail irregularities and spatial variability of support)
- 2. Dynamic train-track interaction analysis
- 3. Cumulative settlement calculation of the railway track deformation for a specific train loading scenario.

The following sections present a detailed description of the models used for the analysis. All the models presented in this report are part of the ROSE library, and can be found in [2].

The cumulative settlement is used as input for the calculation of the track vibration quality. These results are used to answer the research questions.

2.2 Train-track dynamic analysis

The dynamic deformation of the rail during a train passage and the corresponding dynamic forces exerted by the sleepers on the ballast, are computed by means of a dynamic traintrack interaction model. Figure 2.1 shows a schematic representation of the model. This model was presented and described in detail in [3]. This section provides a short description of the model.

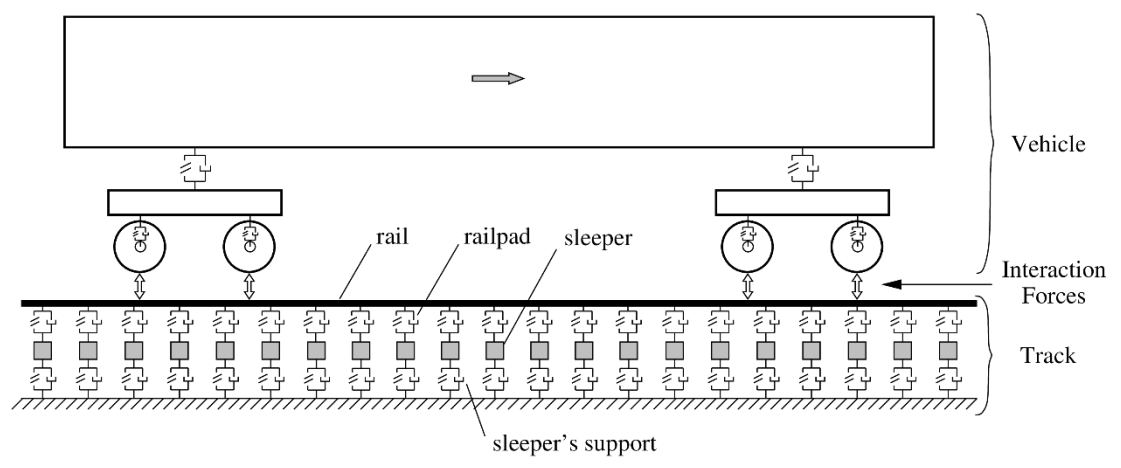


Figure 2.1 Schematic representation of the train-track interaction model [4].

The railway vehicle is modelled as an assembly of rigid bodies connected by linear springs and dampers representing the suspension systems. Figure 2.2 shows the vehicle model considered in this work. Conventional trains are represented by a ten degrees-of-freedom (dof) system.

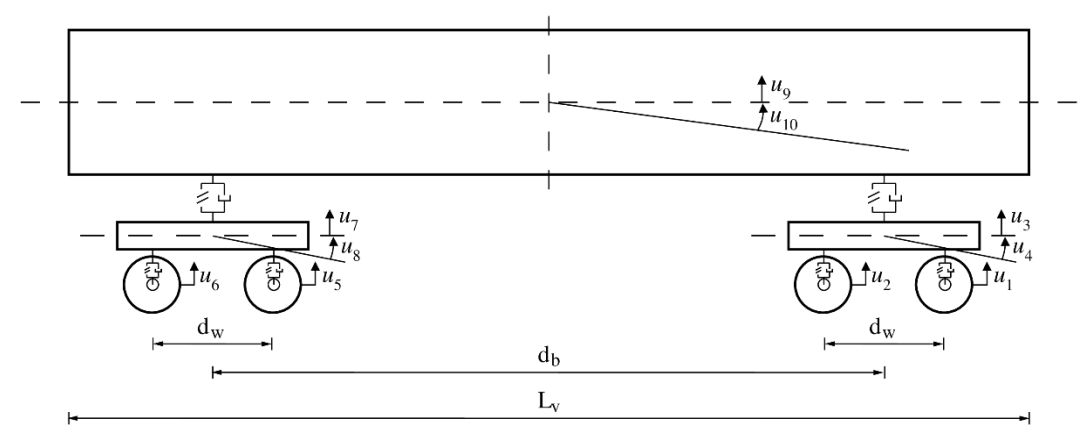


Figure 2.2 Vehicle model with 10 dof [4].

The track is represented by a Winkler type model, assuming that the track is symmetric along its longitudinal axis, where the rail is discretely supported by the sleepers. The rail is described by a classical finite element approach, considering a Euler-Bernoulli beam with discretised mass. The sleepers are represented by lumped masses evenly spaced 0.60~m apart. The support reaction of the sleepers, representing the ballast and subsoil, is given by spring-damper elements, as shown in Figure 2.1. In order to consider hanging sleepers, the support takes place only if there is contact between the base of the sleeper and the ballast, resulting in a non-linear contact model [3].

The vehicle and track systems are coupled through the interaction forces between the wheels and the rails. These forces are determined using the non-linear Hertzian contact theory for metals [5]:

$$F_{w,i} = k_c \delta_i^{1.5}, \tag{1}$$

where k_c is a generalised stiffness coefficient and δ_j is the indentation for wheel j. The indentation δ_i is calculated as:

$$\delta_j = u_{v,j} - u_{t,j} \tag{2}$$

where $u_{v,j}$ is the displacement of wheel j and $u_{t,j}$ is the displacement of the rail at the position of wheel j.

Time integration was performed with a direct explicit method, presented in [6]. The required time-step size was approximately 2.5×10^{-5} s.

2.3 Rail irregularities

2.3.1 Vertical profile rail

The vertical irregularities presented in the rail are expressed following the methodology presented in [7]. The power spectral density of the rail irregularities $S(\Omega)$ is used to produce the samples of the irregularities.

$$S(\Omega) = \frac{2\pi A_v \Omega_c^2}{(\Omega^2 + \Omega_c^2)\Omega^2}$$
(3)

where Ω the wave number, A_{v} the rail irregularity parameter and Ω_{c} is the critical wavenumber. In this analysis, we consider A_{v} =3.365 mm²rad/m, Ω_{c} =0.8242 rad/m, which corresponds to a high-quality railway track, according to the definition of the American Railway Standard [8]. The sample of rail irregularities can be produced by inverse Fourier transform shown as follows:

$$r(x) = \sum_{n=1}^{N} \sqrt{4S(\omega_n)\Delta\omega} \cos(\omega_n x - \theta_n)$$
 (4)

where ω_n , is a circular frequency within the interval in which the PSD function is defined, θ_n , a random phase angle uniformly distributed from 0 to 2π , and $\Delta\omega$ is defined as $(\omega_{\max} - \omega_{\min})/N$, N is the total number of frequency increments in the range ω_{\min} , ω_{\max} .

2.3.2 Rail joints

The modelling of rail joints follows the methodology presented in [9]. The rail join is modelled as a semi-rigid joint with an additional mass. Figure 2.3 shows the representation of the model. This model does not account for the existence of local irregularity at the location of the joint.

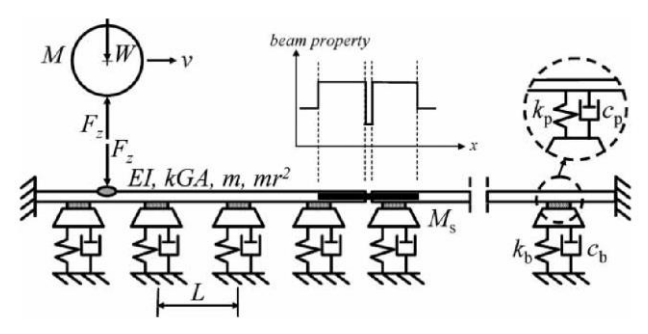


Figure 2.3 Representation of the model to simulate rail joints [9].

2.4 Subsoil dynamic stiffness and damping

The dynamic soil spring stiffness and dashpot damping, that are required for the dynamic train-track analyses, were computed by means of a semi-analytical cone model based on one-dimensional wave propagation [10]. This model assumes that the load is applied to a disk at the surface, which induces stresses on an area that increases with depth; the displacements are constant at the cross section of the cone. Discontinuities can be modelled by assuming at the interface between two layers that one cone leads to the creation of two new cones: reflected and refracted. This allows the modelling of multi-layered soils. The cone method has been extensively applied, because it has the advantage of providing an accurate numerical solution with limited computational efforts [11]. In the current study, the dynamic stiffness, K_{dyn} and damping, D, follow the definition proposed in [10]:

$$K_{dyn} = \text{Re}(S)$$

$$D = \frac{Im(S)}{\omega}$$
(5)

where S is the dynamic stiffness matrix (complex frequency response function) and ω the angular frequency.

The cone model provides a frequency dependent stiffness and damping that needs to be translated into stiffness and damping values for the dynamic train-track model Figure 2.1). The subsoil stiffness and damping were assumed to have the value at the vehicle passing



frequency, corresponding to the vehicle speed divided by the length of the vehicle (L_v in Figure 2.2. For the subsoil, numerical and experimental work has shown that the dynamic response is governed by the vehicle length, and that the influence of individual wheels and bogies is less pronounced [12]–[14]. The stiffness and damping evaluated by the cone method are applied to the dynamic train-track model per half sleeper, as the railway track is assumed symmetric along the longitudinal axis.

2.5 Cumulative cyclic deformation

This section describes the methodology and the main principles behind the procedure adopted for the calculation of the permanent deformation of ballasted tracks. The procedure uses two distinct but coupled models: a dynamic train-track model, that was presented in the previous section, and a settlement model, that will be described next.

Figure 2.4 shows a schematic view of the methodology. The dynamic train passage simulations give the time history of the loads transferred by each sleeper to the ballast, based on which the maximum sleeper-ballast contact force, F_n , is calculated. These values are subsequently used to determine the permanent deformation (settlement) occurring under each sleeper, which is then accumulated assuming that the sleeper load F_n remains constant, following the non-linear evolution described by the settlement model described next, until a limit value of 0.15~mm is attained at a given sleeper. At this point, the contact position of the sleepers with the ballast in the track model is updated and the track superstructure (rails and sleepers) is re-positioned above the ballast bed, under the action of its self-weight. The following passages of the trains are then computed with an updated longitudinal rail level, which will possibly lead to a different distribution of forces transmitted to the ballast, due to the dynamic train-track interaction. The process continues until the required total number of cycles is achieved.

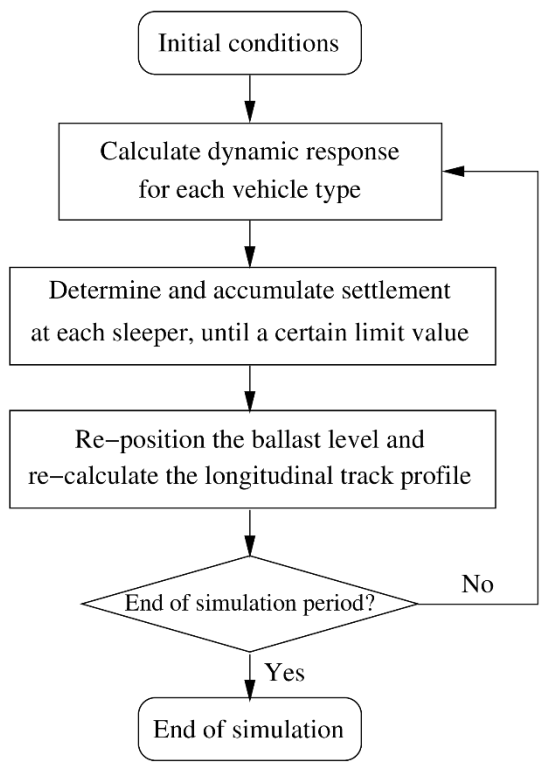


Figure 2.4 Methodology for calculation of railway track cyclic deformation (adapted from [15]).

Figure 2.5 shows the validation of the methodology and of the models adopted for the calculation of the permanent deformation. This validation was performed on a track section over a box culvert near the city of Gouda, in the Netherlands, as described in [15]. The figure shows the agreement between the longitudinal rail level that was measured with topographical equipment with the rail level calculated using the proposed numerical procedure, considering 210 days of service.

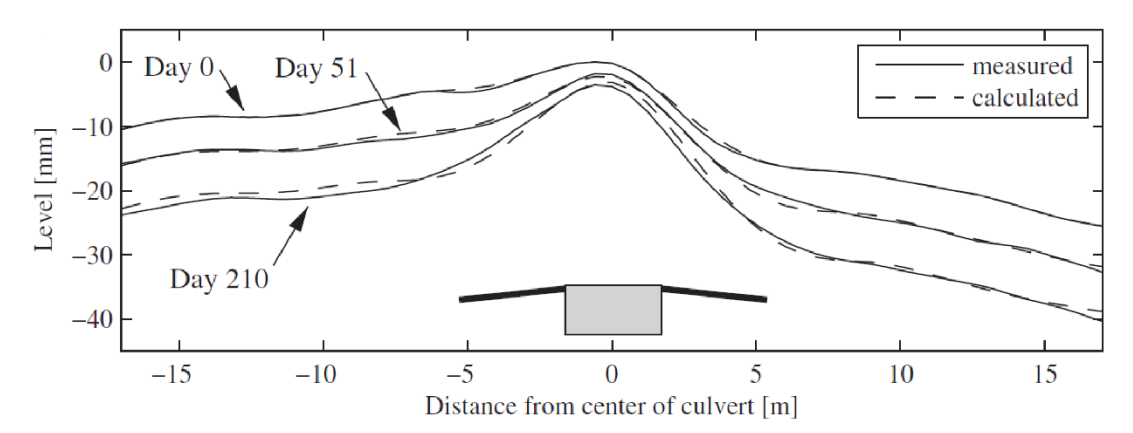


Figure 2.5 Validation of the adopted procedure for settlement calculation [15].

The settlement model consists of two models:

- Model for the ballast settlement.
- · Model for the subsoil settlement.

The total settlement corresponds to the summation of the ballast settlement $(S_{N,b})$ and subsoil settlement $(S_{N,s})$:

$$S = S_{Nh} + S_{NS} \tag{6}$$

2.5.1 Model ballast settlement

The ballast settlement model was inspired by the ballast settlement prediction models presented by Shenton [16], Sato [17] and Ford [18]. The consideration of only the inelastic ballast response is admissible, because normally the permanent vertical deformation of railway tracks is the result of cumulative cyclic deformation that is experienced mainly by the ballast layer [19]. The model was developed to determine the ballast settlement when subjected to an arbitrary loading sequence, making it adequate to be integrated in a vehicle-track interaction model.

In the following, settlements refer to the cyclic accumulation of the tamped track only, although it is known that during the stabilisation of the ballast material, that takes place immediately after construction and during regular tamping operations, a rapid settlement occurs as ballast re-densifies into a more compact state (re-arrangements of the ballast particles to re-establish the required load-bearing structure). The settlements of the tamped track are due to continued densification of the ballast, infiltration of the ballast in the subballast or subgrade, volume reduction from particle breakdown and abrasion, and lateral or longitudinal movement of the ballast particles [20]–[22]. Some authors, as e.g. Sato [17], further separate the settlements of the tamped track in an early phase of rapid settlement and a second phase of lower densification rate. The settlement model described here covers both phases of the tamped-track's settlement.

The settlement of the ballast is proportional to the amplitude of the applied load and the densification of ballast decreases with an increasing number of load cycles, if the loading amplitude remains constant. The model also considers the loading history occurring at each sleeper, making it suitable to be applied at non-homogeneous cases, as transition zones. The permanent deformation of the surface of the ballast under each sleeper caused by each loading cycle (which corresponds to each passing axle), $u_{\{n\}}$, is calculated according to:

$$u_{n} = \frac{\gamma}{M_{\alpha\beta}} \int_{0}^{\overline{F_{n}}} F^{\alpha} \left(\frac{1}{h(F) + 1}\right)^{\beta} dF \tag{7}$$

The total settlement after N load cycles, $S_{N,b}$, is the result of the accumulation of these discrete values:

$$S_{N,b} = \sum_{n=1}^{N} u_n \tag{8}$$

In Equation (7), F is the force, $\overline{F_n}$ is the amplitude of the force passing from the sleeper to the ballast at load cycle n, h(F) represents the loading history, α , β and γ are positive material parameters, and $M_{\alpha\beta}$ is a normalising parameter. The integral in Equation (7) is evaluated numerically.

The value of $\overline{F_n}$ per sleeper results from the dynamic calculation. The ballast material parameters, α , β and γ essentially depend on the ballast intrinsic properties, the initial void ratio of ballast, the size and type of sleepers, the ballast height, and the ballast support condition. These parameters must be determined based on data collected from field or laboratory observations.

The parameter α expresses the dependence of the ballast settlement on the loading amplitude $\overline{F_n}$. For the purpose of the current work, the value α =0.6 was used, resulting from tests performed with different axle load amplitudes [23], and therefore $S_N \propto \overline{F}^{1.6}$. The parameter β controls the progression of the ballast settlement rate with the number of load cycles. In this work, the value β =0.82 was used, which leads to a progression of settlement with the number of load cycles similar to Shenton's settlement model [16], as was demonstrated in [15]. The Shenton's settlement model is sound because it was derived based on available field data from worldwide sources.

Parameter $M_{\alpha\beta}$ is defined by:

$$M_{\alpha\beta} = \frac{F_0^{\alpha+1}}{\alpha+1} \sum_{n=1}^{N_0} \left(\frac{1}{n}\right)^{\beta},\tag{9}$$

where F_0 is a reference loading amplitude and N_0 a reference number of cycles. To discuss the meaning of parameter $M_{\alpha\beta}$, as well as of γ , Equation (7) is simplified for the constant loading case: considering the constant loading amplitude as \bar{F} , then the function h(F) can be replaced by the number of cycles passed (n-1) and Equation (7) simplifies to:

$$u_{p,n} = \frac{\gamma}{M_{\alpha\beta}} \frac{\overline{F^{\alpha+1}}}{(\alpha+1)} \left(\frac{1}{n}\right)^{\beta} \tag{10}$$

and the corresponding accumulated settlement is then given by:



$$S_{N,b} = \frac{\gamma}{M_{\alpha\beta}} \frac{\overline{F^{\alpha+1}}}{(\alpha+1)} \sum_{n=1}^{N} \left(\frac{1}{n}\right)^{\beta}$$
 (11)

By comparing Equations(8) with (10), it can be seen that $M_{\alpha\beta}$ was derived so that parameter γ represents the accumulated ballast settlement that would occur if the loading amplitude F_0 was applied N_0 cycles. This gives a physical meaning to parameter γ and also offers a way to experimentally estimate this parameter, either by means of specific field measurements or from experimental tests carried out on ballast samples collected at the site. As mentioned in [15], the values $N_0 = 10^6$ and $F_0 = 50$ kN were used. The justification for the value chosen for N_0 is that many tests with ballast, available in the literature, are performed with this total number of load cycles, whereas the value for F_0 is representative of the force transmitted to the ballast through a half-sleeper.

The function h(F) stores the loading history of each sleeper of the model and is updated each time Equation (7) is evaluated. It may be defined as an inverted cumulative histogram of the loading. The value h(F) gives the number of times the loading on a particular sleeper has exceeded the value F, where the loading is defined here as the maximum sleeper-ballast contact force for a given dynamic simulation. This function is automatically calculated and stored by the program.

2.5.2 Model subsoil settlement

The subsoil settlement model is a modified version of that proposed by Li and Selig [24], and modified by Charoenwong *et al.* [25] to account for the evolution of the dynamic stress and to allow the simulation of both newly constructed and existing track. The settlement, S_{Ns} , is computed as follow:

$$S_{Ns} = \sum_{i=1}^{k} \Delta \epsilon_{p_s,i_j} \cdot h_j \tag{12}$$

where $\Delta \epsilon_{p_{_}s,i_j}$ and h_j represent, respectively, the subsoil permanent strain increment and the thickness of layer j. The permanent strain increment follows:

$$\Delta \epsilon_{p_{\underline{s}},i_{j}} = \frac{a}{100} \left(\frac{\sigma_{d_{s},i}}{\sigma_{s}} \right)^{m} \left[\left((dN \cdot i) + N_{1s} \right)^{b} - \left(\left(dN \cdot (i-1) \right) + N_{1s} \right)^{b} \right]$$

$$(13)$$

where $\sigma_{d_{s,i}}$ is the subsoil dynamic deviatoric stress relevant to the traffic load, σ_s is the compressive strength, N_{1s} is the number of load cycles after the last subsoil replacement and a, m and b are materials parameters given in Table 2.1.

Table 2.1 Settlement parameters for various subsoil types [24].

Material parameter	High plasticity clay	Low plasticity clay	High plasticity silt	Low plasticity silt
а	1.20	1.10	0.84	0.64
b	0.18	0.16	0.13	0.10
m	2.40	2.00	2.00	1.70



2.6 Spatial variability

The spatial variability has been modelled by means of random fields. Random fields are commonly used to model the spatial variability of soil properties. Within this study, spatial variability is considered for the stiffness, K_s (stiffness of the ballast and subsoil system), with all other soil properties being assumed constant.

In this study structured random fields are generated using GSTools v1.3, a geostatistical modelling toolkit [26]. Within the toolkit isotropic and anisotropic spatial random fields based on a given covariance, or correlation, function are generated using the randomisation method [27-28].

For this study an exponential correlation function is used to generate the random fields. The random fields are initially generated follow an ordinary Gaussian distribution, in that its point statistics follow a normal distribution with a mean, $\mu=0$, and a standard deviation, $\sigma=1$. This distribution is unrealistic for soil properties, and therefore this field is transformed to a distribution more representative of the soil that is modelled. For the purposes of this study, a lognormal distribution is chosen, which is typical for stiffness properties in geomaterials, as it usually provides a good fit while removing physically implausible negative values.

The variability is accounted for by assuming that the stiffness and damping follow a lognormal distribution, so that $ln(K_s)$ and $ln(C_s)$ are represented by a normally distributed random field, described by the point statistics, mean, $\mu_{ln(X)}$ and standard deviation, $\sigma_{ln(X)}$; while the spatial statistics, the horizontal scale of fluctuation (θ), describe the spatial variation in the soil properties field. In the forthcoming analysis the variability in the soil properties is modelled by means of the Coefficient of Variation ($COV = \sigma/\mu$). This value is assumed to be 25%, which is in agreement with the COV that are expected for CPT tip resistances [29]. The horizontal scale of fluctuation is assumed to be $\theta = 20$ m, which is in the range of typical values [30].

2.7 Track vibration quality parameters

The calculation method for the track vibration quality parameters H_{max} and H_{rms} have been provided by Level Acoustics & Vibration in the form of a matlab script. This script has been used in this report to compute the H_{max} and H_{rms} parameters.



3 Case study description

3.1 Analyses description

The analysis has been performed for four different scenarios:

- S1. Transition zone from soft to stiff subsoil.
- S2. Transition zone from stiff to soft subsoil.
- S3. Rail joint on soft subsoil.
- S4. Rail joint on stiff subsoil.

For the analyses the A2 corridor (Amsterdam - Eindhoven) was chosen as an example to derive realistic train loadings and subsoil parameters. The analyses are performed in a soft and stiff subsoil. The subsoil corresponds to the soil layers that are below the ballast. The ballast layer was considered to be the same for both types of subsoil schematisations.

3.1.1 Transition zone

Transition zones are part of the railway track structure and are characterised by an abrupt change in track support stiffness which leads to deterioration of the vertical track geometry and even to damage of the track components [31]. In consequence, transition zones have high maintenance demands required to keep the track at the desired geometry for ensuring passenger ride comfort and to avoid speed restrictions [32].

The transition zone that it is modelled in the forthcoming analysis is a simplification of a transition zone, and corresponds to an abrupt change in stiffness of the subsoil. The railway track (rail, railpads, sleepers and ballast) along the transition zone is constant, and the variation in stiffness occurs abruptly from either soft to stiff or stiff to soft subsoil. Figure 3.1 shows the schematic representation of the transition zone.

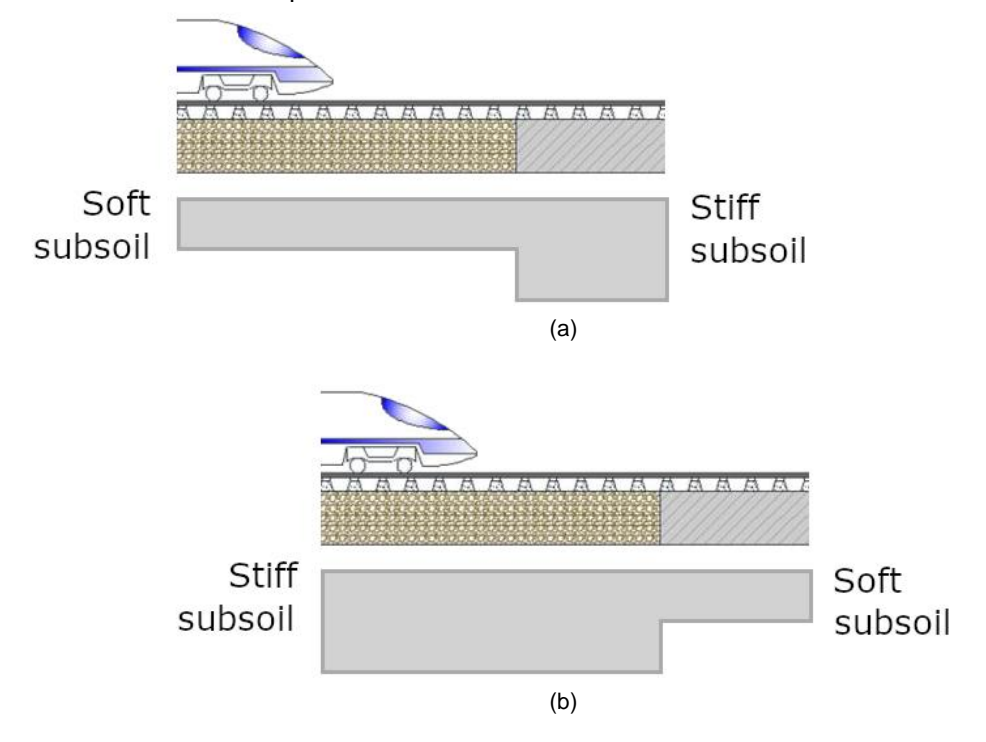


Figure 3.1 Representation of the transition zone: (a) from soft to stiff subsoil and (b) from stiff to soft subsoil.

3.1.2 Rail joint

Rail joints are used to electrically section the railway track. When the train is passing a joint and entering a section, it creates a short-cut that triggers a signal indicating that no other train can enter the same track section. When the train passes the next insulated joint, the passed track section is deblocked for the following train.

In this study the rail joint properties follow ProRail specifications [33]. The mass of the rail joint is 60 kg and the stiffness of the rail joint is 95% of the rail in the downward direction, and approximately 85% of the rail in the upward direction. In the forthcoming analysis a constant value of 90% is used for the stiffness of the rail joint.

3.2 Subsoil description and characterisation

3.2.1 Subsoil description

The subsoil properties have been derived from the Stochastic Subsoil Schematisation (SoS) that it is available for the A2 Corridor. The chosen locations are in the vicinity of Maarssen (see Figure 3.2). The soft subsoil corresponds to scenario 4 of the segment 1079, whilst the stiff subsoil corresponds to scenario 2 of segment 1077.

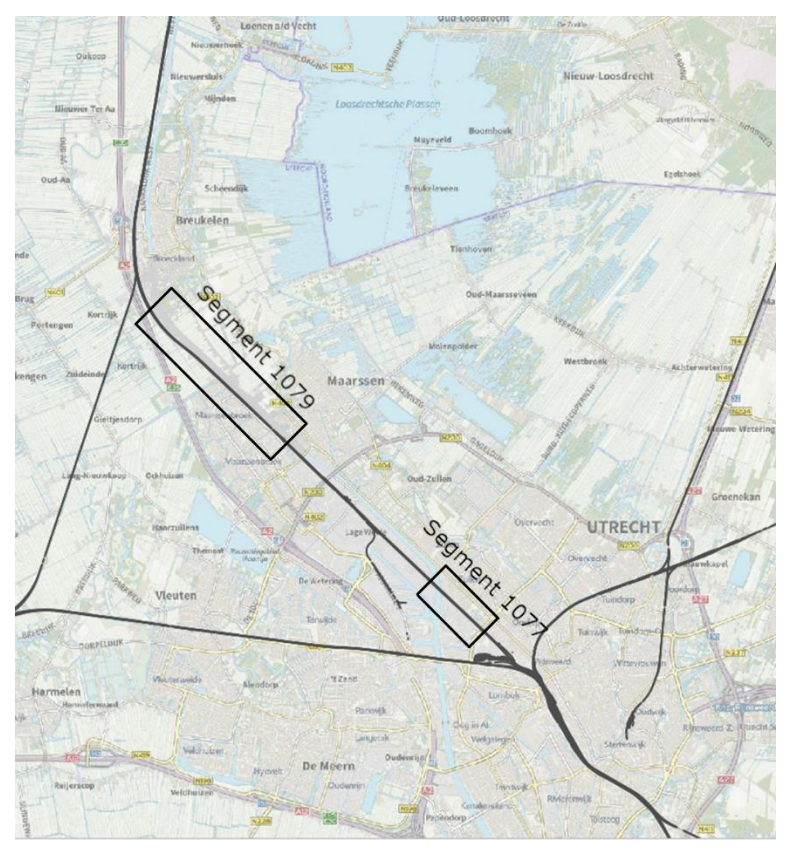


Figure 3.2 Location of the SOS segments along the A2 corridor.

Figure 3.3 shows the layering of the soft and stiff subsoils. The properties of the different soil layers, and its lithological description can be found in Table A.1 in Appendix A. The parameters for the cumulative analysis have been described in §2.5.

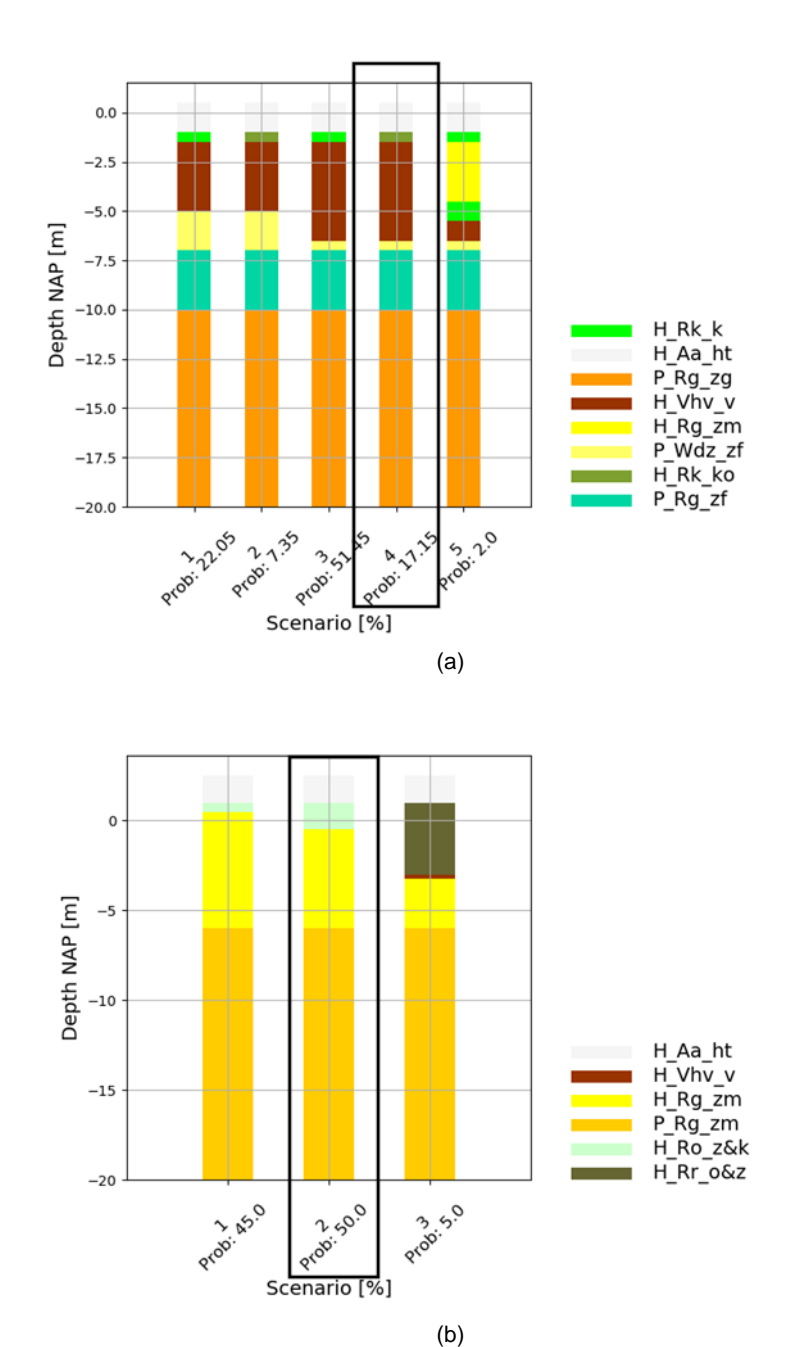


Figure 3.3 Subsoil layering for: (a) soft subsoil (scenario 4) and (b) stiff subsoil (scenario 2).

3.2.2 Subsoil characterisation

The subsoil dynamic stiffness and damping have been computed following the methodology presented in §2.4. Figure 3.4 shows the dynamic stiffness and damping for the soft and stiff subsoils.

The expected dominant frequency for regular trains ranges between 1 and 3 Figure 3.4Figure 200 800 150 600 K_{dyn} [MN/m²] C_{dyn} [kNs/m] 400 100 200 0 15 Frequency [Hz] 15 Frequency [Hz] (a) 1000 200 800 K_{dyn} [MN/m²] C_{dyn} [kNs/m] 100 400

3.4

Figure 3.4 Dynamic stiffness and damping for the subsoil: (a) soft and (b) stiff subsoils.

Frequency [Hz]

3.3 Railway track

50

0 +

The railway track superstructure consists of continuously welded UIC54E1 rails and monoblock concrete sleepers on top of a ballast bed. The properties for the rail and sleepers are presented in Table 3.1 and Table 3.2, respectively.

200

0+

(b)

15

Frequency [Hz]

Table 3.1 Rail properties for the numerical analysis [32].

Parameter	Value		
Cross section area	6934 mm ² -> 6934 × 10 ⁻⁶ m ²		
Unit weight	77 kN/m³		
Young's modulus	210 × 10 ⁶ kPa		
Moment of inertia around the second axis (I ₂)	2.127 × 10 ⁻⁵ m ⁴		
Moment of inertia around the third axis (I ₃)	2.127 × 10 ⁻⁵ m ⁴		

Table 3.2 Sleeper properties for the numerical analysis.

Parameter	Value	
Sleeper type	NS90 sleepers	
Weight	285 kg	
Centre-to-centre spacing	600 mm	

3.4 Ballast

The ballast is assumed to have a thickness of 0.50 m. The remaining elastic material properties are shown in Table 3.3.

Table 3.3 Ballast properties for the numerical analysis [34].

Parameter	Value		
Young's modulus	200× 10 ³ kPa		
Poisson ratio	0.2		

3.5 Train loading scenarios

The train traffic used to compute the railway track degradation is based on the Gotcha information available at a station located along the A2 corridor, for the year of 2019.

3.5.1 Passenger trains

The number and types of passenger train are easily derived from the overview of the Gotcha data. In average, the railway line is loaded every hour with the following trains (in each direction):

- 6 VIRM.
- 3 SLT.
- 1 SGM.

The information about the mass and configuration of the passengers trains can be found in [2]. In the forthcoming analyses it is assumed that the passengers traffic takes place for 16 hours each day, and the travelling speed is constant and equal to 140 km/h.

3.5.2 Freight trains and locomotives

Estimating the average loading due to freight trains is challenging since, in the Gotcha data, there are 47 different train type with more than 8500 different configurations. Performing numerical calculations for all the different train configurations is computationally very demanding.



Figure 3.5 shows the load distribution of the freight trains. It follows that the locomotives and unloaded freight trains have little variation on the force, but the loaded freight trains show a great variability on the loaded force. The force applied by the unloaded wagons is significantly smaller than the force applied by either the loaded freight trains or locomotives.

Figure 3.6 presents the distribution of the locomotives (Figure 3.6a) and loaded freight trains (Figure 3.6 b) along the A2 corridor. It follows that there are certain types of freight trains that load the track more frequently than others. The locomotive types EL BR189, EL BR186 and Lok 1600, correspond to more than 77% of the locomotives travelling along the A2 corridor. The loaded freight train types FALNS5, SGNS1, TAPPS and SGGMRS correspond to more than 67% of the loaded freight train types. Therefore, in the forthcoming analysis, it was considered that the freight trains consist of these four train types, combined with the three locomotives. All the freight traffic is assumed to travel at 80 km/h. The information about the mass and configuration of the freight trains and locomotives can be found in [2].

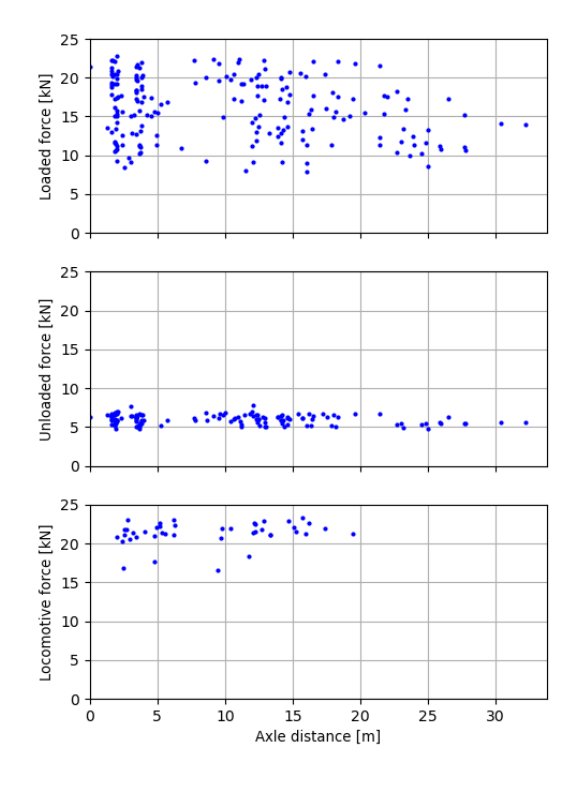


Figure 3.5 Load distribution along the A2 corridor due to freight trains and locomotives.

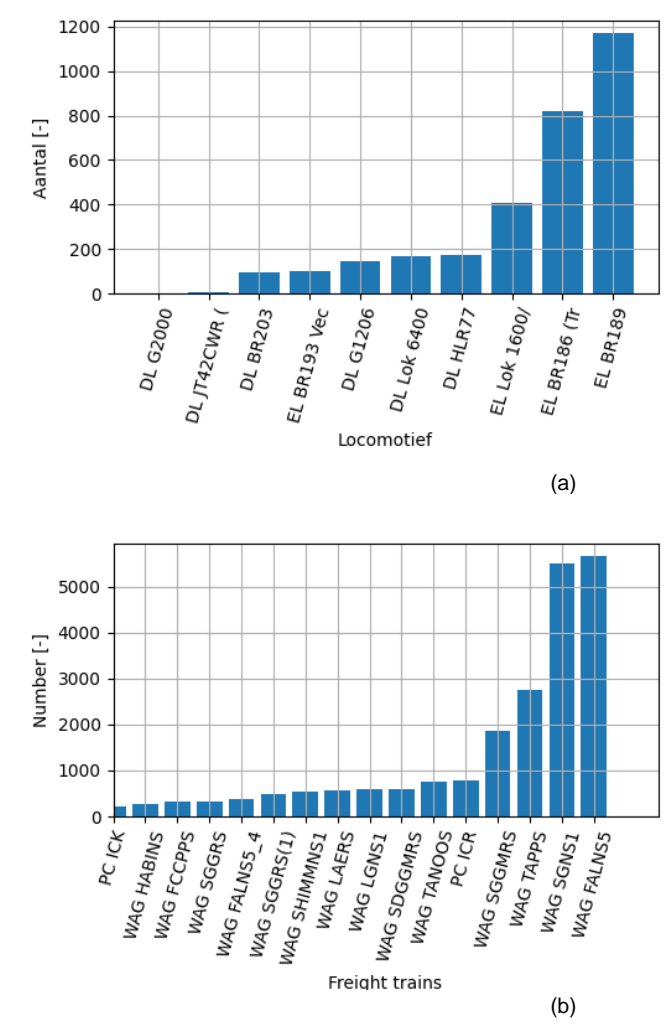


Figure 3.6 Distribution of freight train types: (a) locomotives and (b) loaded freight trains.

4 Results

The results of the numerical analyses will be presented in discussed in the forthcoming sessions. The results correspond to the settlement of the track as a function of the position after four, eight and twelve months (122, 242 and 365 days).

4.1 Transition zone

4.1.1 Soft to stiff subsoil

4.1.1.1 Without irregularities

The results regarding the transition zone spanning between a soft and stiff subsoil are presented in Figure 4.1, for the case where the contact between the train and the rail is perfect, i.e. there are no irregularities. Note that in these figures the settlement is draw in upward direction. The rail is assumed to be placed horizontally along the vertical displacement 0 mm. The results show that initially (after 122 days) the greater displacement occurs at the stiff side of the transition zone. At the time progresses (242 and 365 days), the greatest displacement occurs at the side of the soft side. This difference in behaviour is due to the cumulative model formulation. Initially, the majority of the displacement occurs due to ballast densification (which is greater on the stiff side, because the contact forces between the train and rail are greater on the stiff side – see Figure 4.2). As the time progresses, the densification rate decreases, and the displacement due to creep and plastic deformation of the subsoil starts dominating the response, due to the softer layers that exist on the soft side of the transition zone.

The results around the transition zone also illustrate the displacement is greater close to the transition zone than on the free track further away from the transition zone. These results are in agreement with experimental reports from literature (e.g. [35-36]).

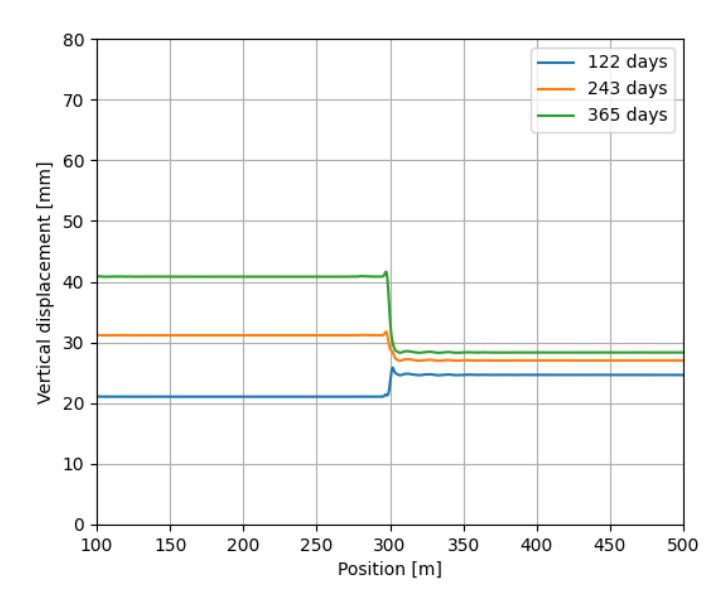


Figure 4.1 Railway track deformation at a transition zone (soft to stiff subsoil), at different moments in time.

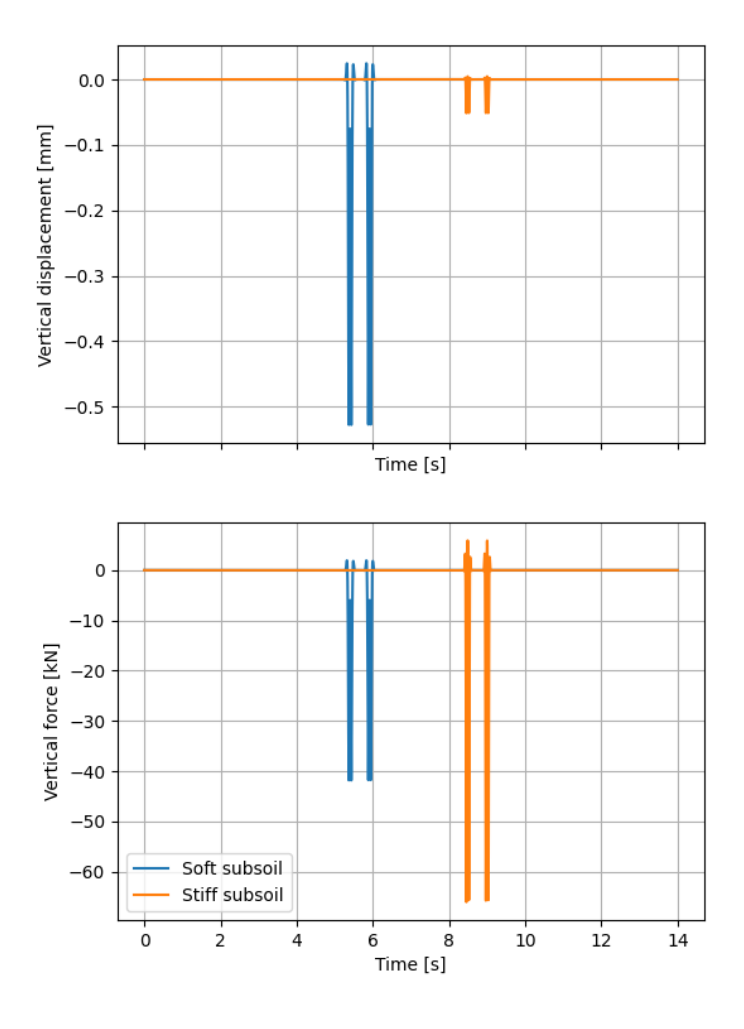


Figure 4.2 Comparison of the dynamic vertical displacement and dynamic contact forces on soft and stiff subsoil during the passage of a VIRM at 140 km/h.

4.1.1.2 Effect of irregularities

The results regarding the transition zone spanning between a soft and stiff subsoil are presented in Figure 4.3, for the case where irregularities are presented (the irregularities are defined in §2.3.1 and corresponds to a high-quality railway track).

The results are similar to the ones obtained for the case without irregularities. The irregularities cause an oscillation of the contact forces that in turn introduces a variability on the displacement along the track. The effect of the irregularities becomes gradually more important as time progresses. For the settlement at 122 days the effect of the irregularities is less pronounced than at 365 days.

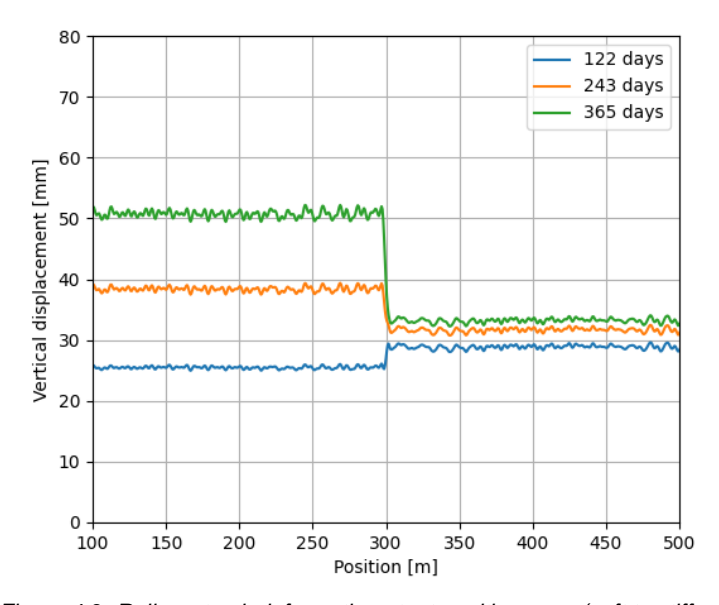


Figure 4.3 Railway track deformation at a transition zone (soft to stiff subsoil), at different moments in time, considering irregularities.

4.1.1.3 Effect of spatial variability

The results regarding the transition zone spanning between a soft and stiff subsoil are presented in Figure 4.4, for the case where irregularities are presented (the irregularities are defined in §2.3.1 and corresponds to a high-quality railway track), and for the case where spatial variability is present (as defined in §2.6).

The figure shows that the effect of spatial variability is significant for the estimation of the railway track deformation. In particular, on the soft subsoil side the spatial variability causes significant variations in the computed displacement. This variation is much more significant for the track deformation than the variation introduced by the rail irregularities.

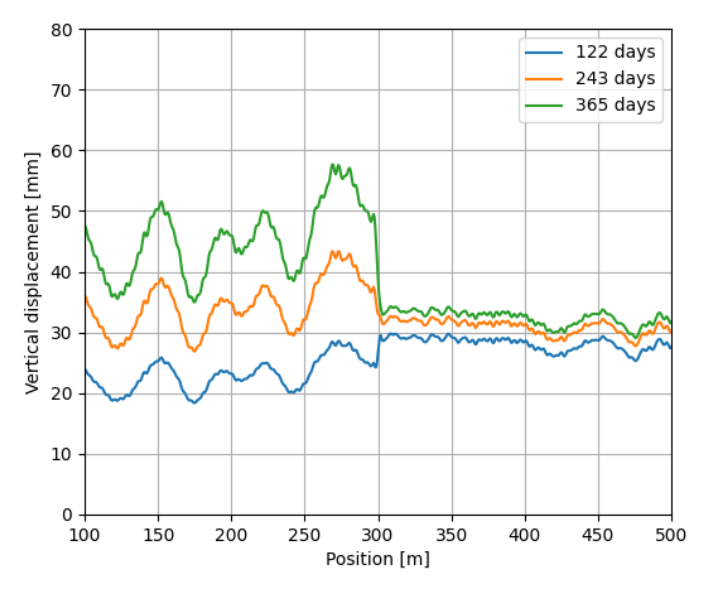


Figure 4.4 Railway track deformation at a transition zone (soft to stiff subsoil), at different moments in time, considering irregularities and spatial variability.

4.1.2 Stiff to soft subsoil

4.1.2.1 Without irregularities

The results regarding the transition zone spanning between a stiff and soft subsoil are presented in Figure 4.5, for the case where the contact between the train and the rail is perfect, i.e. there are no irregularities.

Similar to the transition zone from soft to stiff subsoil, the results show that initially (after 122 days) the greater displacement occurs at the stiff side of the transition zone. At the time progresses (242 and 365 days), the greatest displacement occurs at the side of the soft side.

The results around the transition zone also illustrate the displacement is greater close to the transition zone than on the free track further away from the transition zone. This is clear on the soft side of the transition zone.

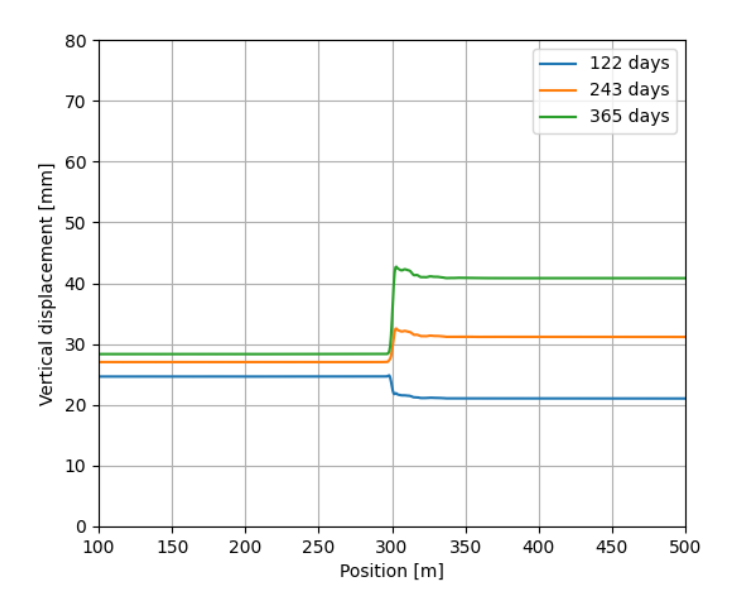


Figure 4.5 Railway track deformation at a transition zone (stiff to soft subsoil), at different moments in time.

4.1.2.2 Effect of irregularities

The results regarding the transition zone spanning between a stiff and soft subsoil are presented in Figure 4.6, for the case where irregularities are presented (the irregularities are defined in §2.3.1 and corresponds to a high-quality railway track).

The results are similar to the ones obtained for the case without irregularities, and the conclusions are the same as presented for the transition zone from soft to stiff subsoil.



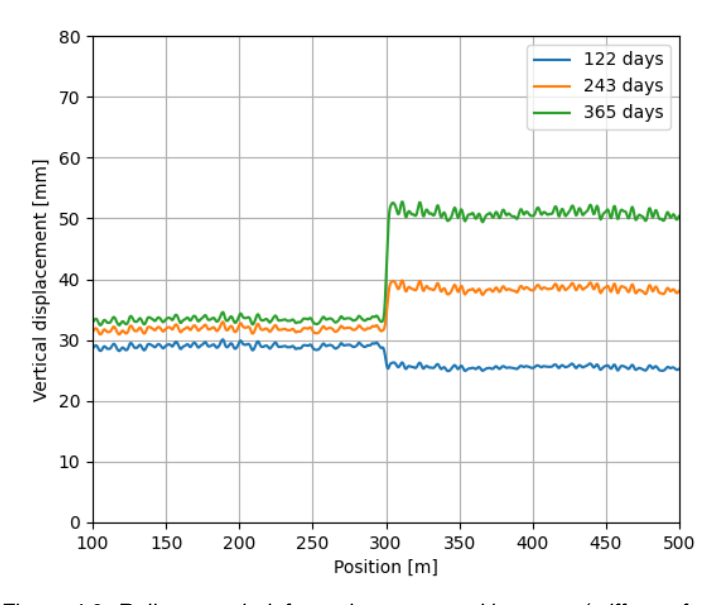


Figure 4.6 Railway track deformation at a transition zone (stiff to soft subsoil), at different moments in time, considering irregularities.

4.1.2.3 Effect of spatial variability

The results regarding the transition zone spanning between a stiff and soft subsoil are presented in Figure 4.7, for the case where irregularities are presented (the irregularities are defined in §2.3.1 and corresponds to a high-quality railway track), and for the case where spatial variability is present (as defined in §2.6).

Again, it is highlighted the importance of spatial variability for the estimation of the railway track deformation. In particular on the soft subsoil side the spatial variability of the subsoil causes significant variations in the computed displacement. This variation is much more significant than the variation introduced by the rail irregularities.

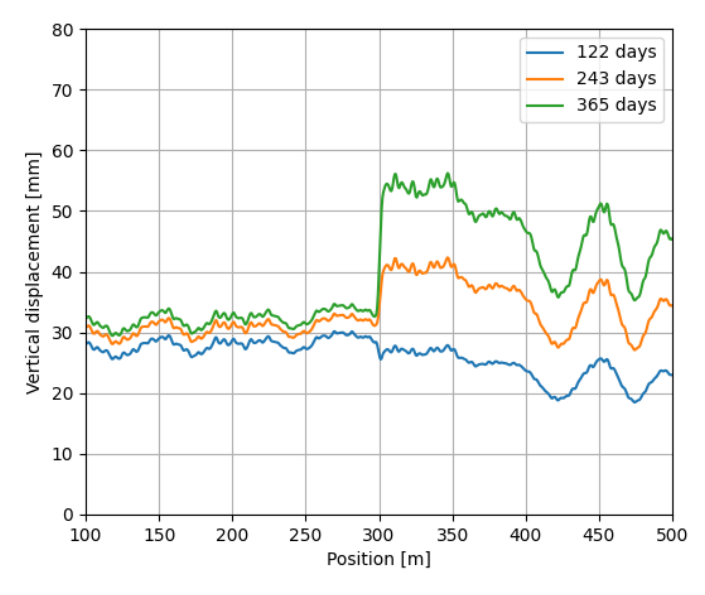


Figure 4.7 Railway track deformation at a transition zone (stiff to soft subsoil), at different moments in time, considering irregularities and spatial variability.

4.2 Rail joint

4.2.1 Soft subsoil

4.2.1.1 Without irregularities

The results regarding the rail joint on the soft subsoil are presented in Figure 4.8, for the case where the contact between the train and the rail is perfect, i.e. there are no irregularities. The results show that there is a small amplification of the vertical displacement on the location of the rail joint. However, the dynamic amplification on the rail joint is very small. This is related to the fact that the bending stiffness of the rail joint is very high (90% of the bending stiffness of the rail). This is further illustrated in Figure 4.9, which compares two bending stiffness reduction factors for the rail joint: 60% and 90%, during the passage of a VIRM train at 140 km/h. The results show that when considering a 60% reduction of the bending stiffness both the displacement and contact force increase.

It should be highlighted that the main effect of the rail joint is likely to occur at high frequencies (> 500 Hz), which are not relevant for railway track deformation [9].

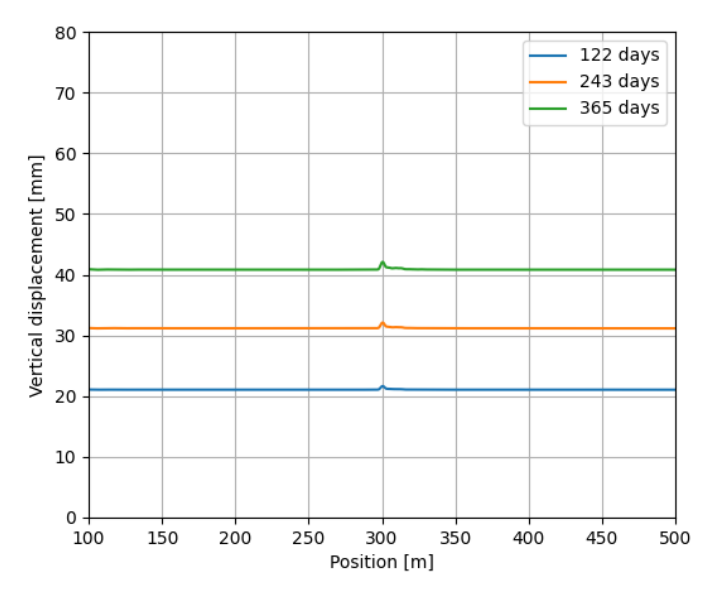


Figure 4.8 Railway track deformation at a rail joint (on soft subsoil), at different moments in time.

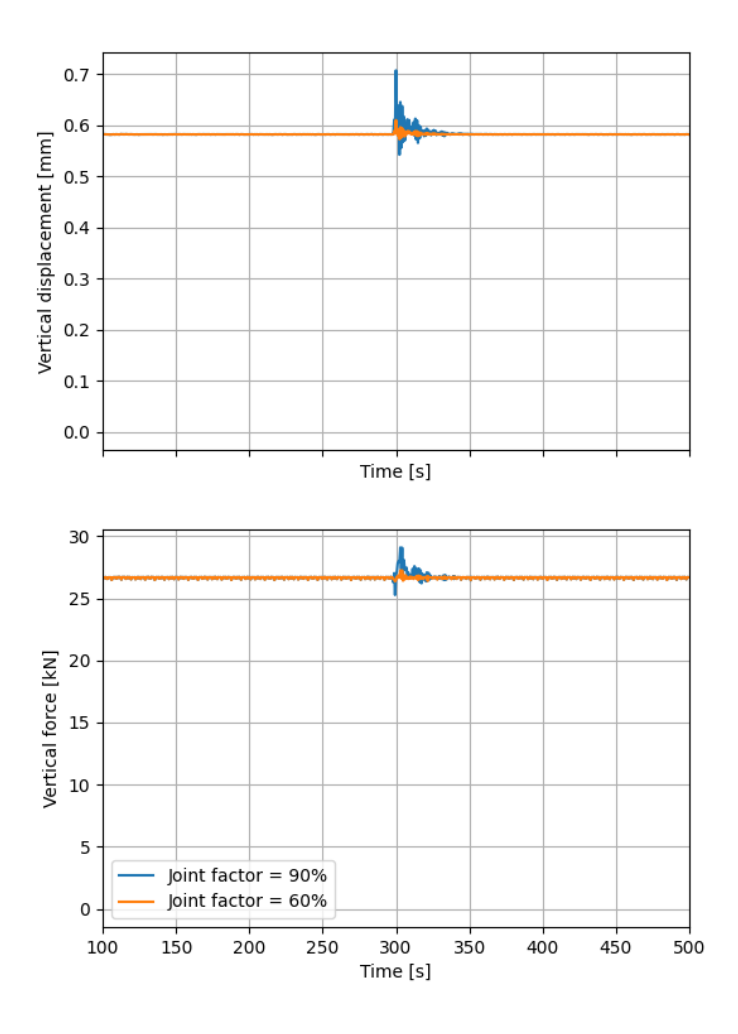


Figure 4.9 Effect of the stiffness of the rail joint on the vertical displacement and contact force during the passage of a VIRM at 140 km/h.

4.2.1.2 Effect of irregularities

The results regarding the rail joint on the soft subsoil are presented in Figure 4.10, for the case where irregularities are presented (the irregularities are defined in §2.3.1 and corresponds to a high-quality railway track).

For the cumulative settlement, the presence of rail irregularities overshadows the effects caused by the rail joint. The variations in the contact introduced by the irregularities are in the same order of magnitude as the ones introduced by the rail joint, and therefore it is no longer possible to identify the rail joint.

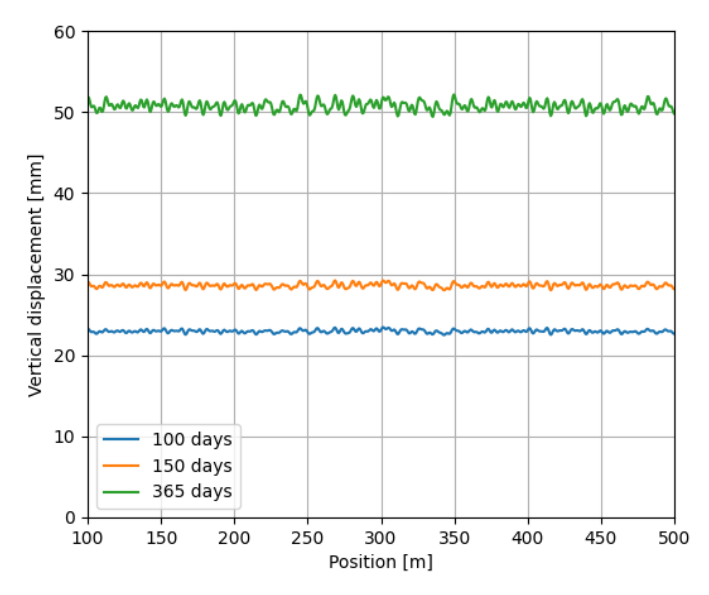


Figure 4.10 Railway track deformation at a rail joint (on soft subsoil), at different moments in time, considering irregularities.

4.2.1.3 Effect of spatial variability

The results regarding the rail joint on the soft subsoil are presented in Figure 4.11, for the case where irregularities are presented (the irregularities are defined in §2.3.1 and corresponds to a high-quality railway track), and for the case where spatial variability is present (as defined in §2.6).

When spatial variability is present, the rail joint becomes indistinguishable, similar to the case of irregularities. The variation in the displacement along the railway track is governed by the spatial variability.

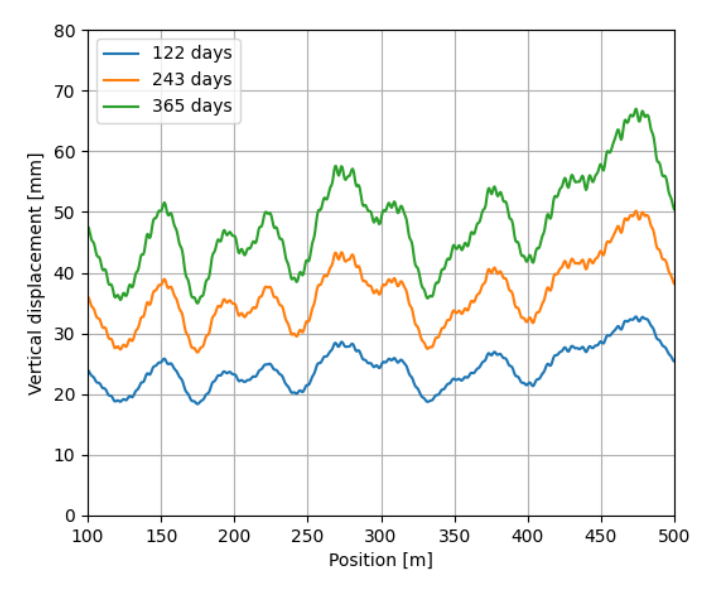


Figure 4.11 Railway track deformation at a rail joint (on soft subsoil), at different moments in time, considering irregularities and spatial variability.

4.2.2 Stiff subsoil

4.2.2.1 Without irregularities

The results regarding the rail joint on the stiff subsoil are presented in Figure 4.12, for the case where the contact between the train and the rail is perfect, i.e. there are no irregularities.

Similar to the rail joint on soft subsoil, the results show that the rail joint effect is very small on the accumulative displacement that develops in time.

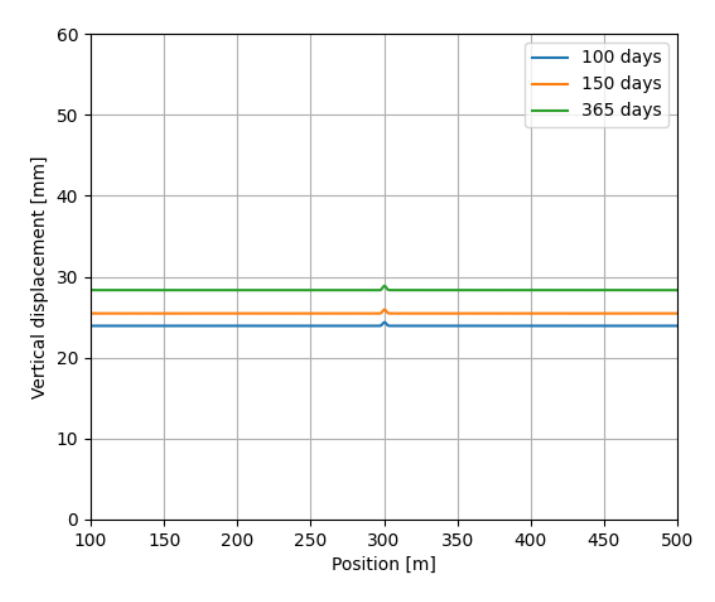


Figure 4.12 Railway track deformation at a rail joint (on stiff subsoil), at different moments in time.

4.2.2.2 Effect of irregularities

The results regarding the rail joint on the stiff subsoil are presented in Figure 4.13, for the case where irregularities are presented (the irregularities are defined in §2.3.1 and corresponds to a high-quality railway track).

Again, it is found that, for the cumulative settlement, the presence of rail irregularities overshadows the effects caused by the rail joint. The variations in the contact introduced by the irregularities are in the same order of magnitude as the ones introduced by the rail joint, and therefore it is not possible to identify the rail joint.



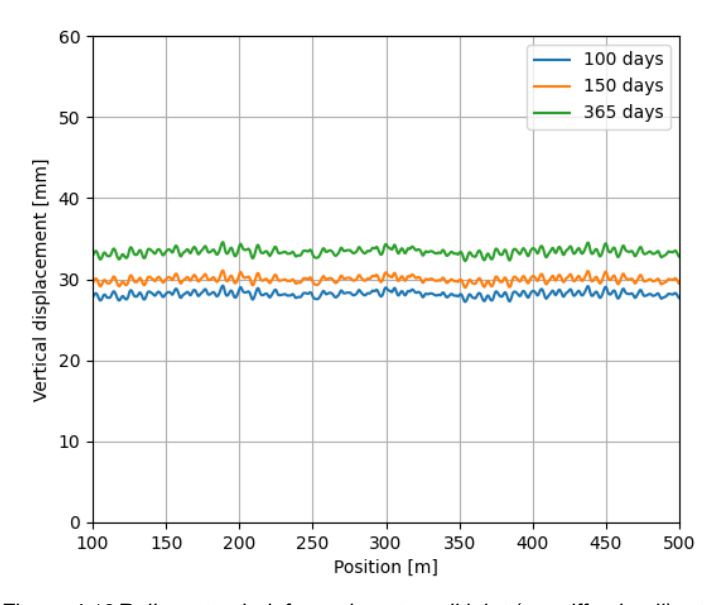


Figure 4.13 Railway track deformation at a rail joint (on stiff subsoil), at different moments in time, considering irregularities.

4.2.2.3 Effect of spatial variability

The results regarding the rail joint on the stiff subsoil are presented in Figure 4.14, for the case where irregularities are presented (the irregularities are defined in §2.3.1 and corresponds to a high-quality railway track), and for the case where spatial variability is present (as defined in §2.6).

Again, it is highlighted the importance of spatial variability for the estimation of the railway track deformation. The variation introduced by the spatial variability is much more significant than the variation introduced by the rail irregularities.

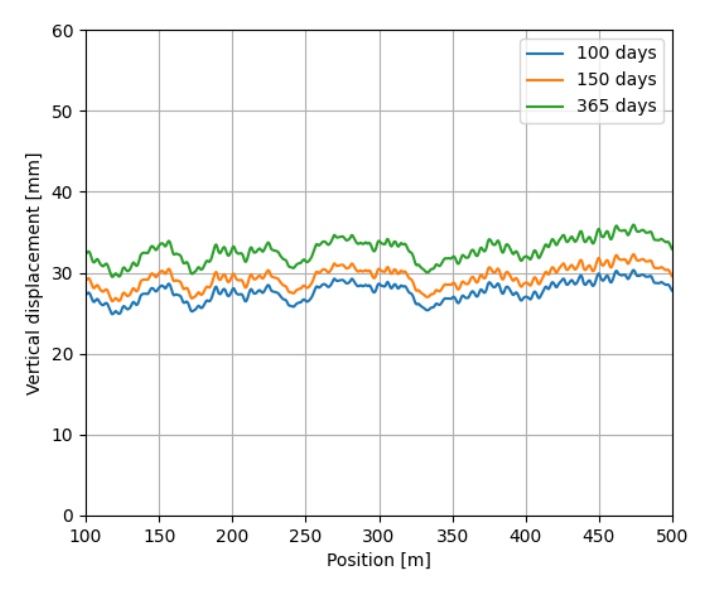


Figure 4.14 Railway track deformation at a rail joint (on stiff subsoil), at different moments in time, considering irregularities and spatial variability.

4.3 H_{max} and H_{rms}

In order to establish a relationship between the railway induced vibration and the railway track geometry, [1] defines two new parameters: H_{max} and H_{rms} . These parameters are computed based on the railway track geometry and try to characterise the track quality concerning the generation of environmental vibration.

In the following section the results of these two parameters will be presented for the case including irregularities and irregularities and spatial variability. A length of 200 m has been used to compute H_{max} and H_{rms} (considering 100 m to the left and 100 m to the right of the point of discontinuity in the track).

4.3.1 Transition zone

4.3.1.1 Soft to stiff subsoil

Figure 4.15 shows the parameters H_{max} and H_{rms} for a transition zone spanning between a soft and stiff subsoil. Figure 4.15a corresponds to the analysis with rail irregularities, while Figure 4.15b corresponds to the analysis with rail irregularities and spatial variability. The analysis show that there is no difference in time for both parameters.

The difference between the two analyses (with and without spatial variability), is further illustrate in Figure 4.16. For the transition zone between a soft and stiff subsoil the difference between the two parameters H_{max} and H_{rms} . is negligible. However, from Figure 4.3 and Figure 4.4 it is clear that both irregularities and spatial variability play a significant role on the railway track deformation in time.

The variation induced by the irregularities and spatial variability is not visible on the two new parameters, likely because they are only defined for wavelengths up to 10 m, while the long-term deformation of the railway track occurs for greater wavelengths.



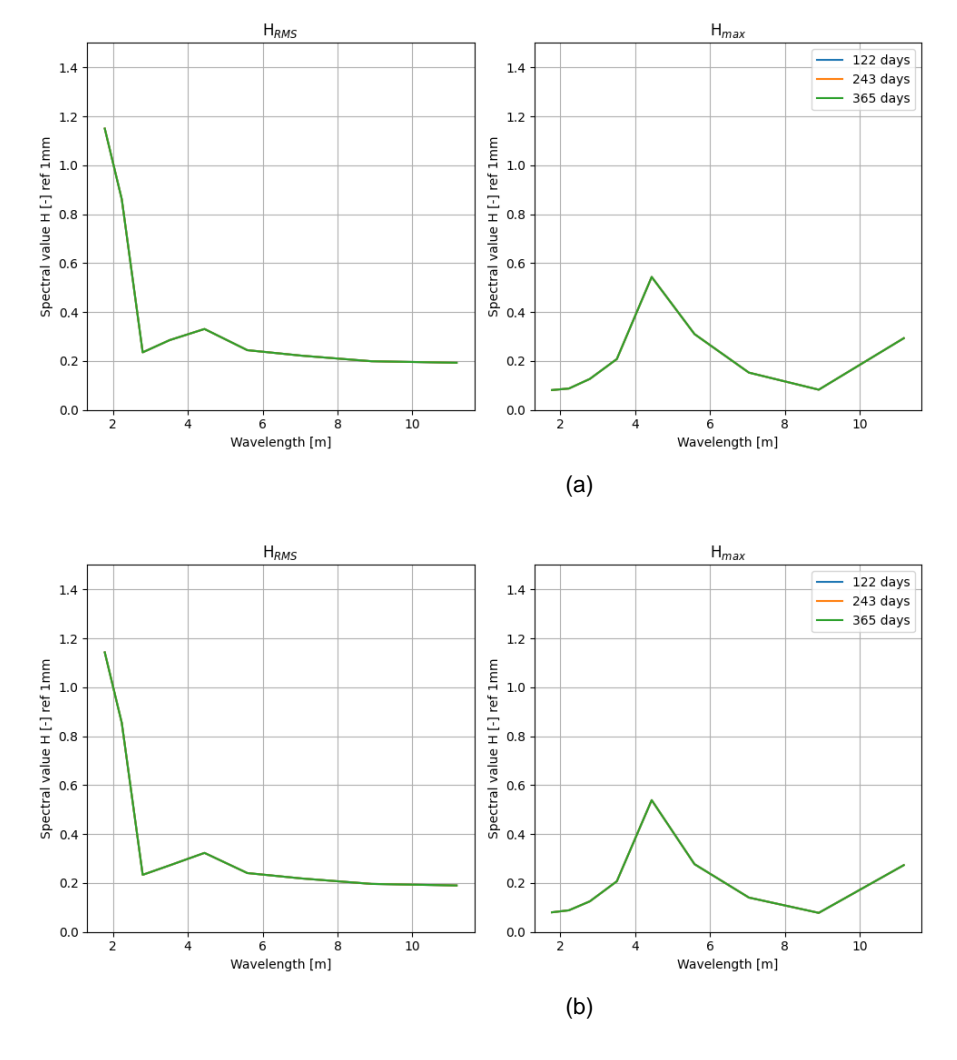


Figure 4.15New parameter H_{max} and H_{rms} at a transition zone (soft to stiff subsoil), at different moments in time, considering: (a) irregularities and (b) irregularities and spatial variability.

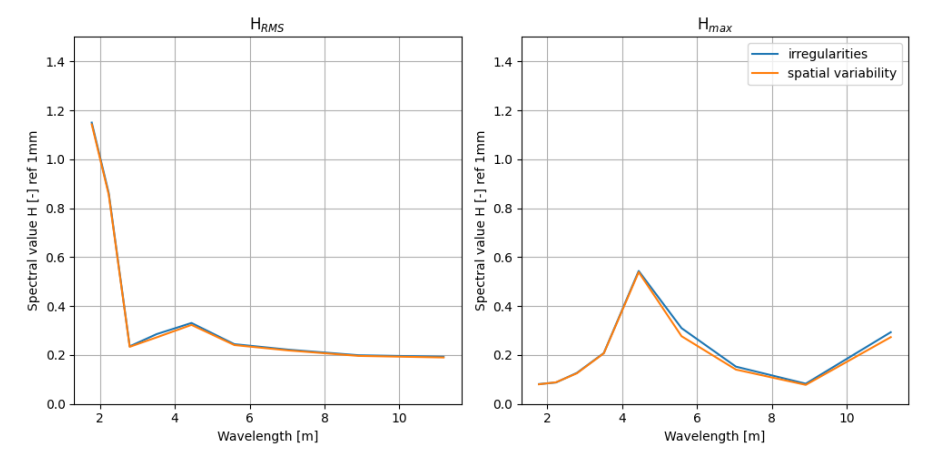


Figure 4.16 New parameter Hmax and Hrms at a transition zone.

4.3.1.2 Stiff to soft subsoil

Figure 4.17 shows the parameters H_{max} and H_{rms} for a transition zone spanning between a stiff and soft subsoil. Similar to the analysis presented in §4.3.1.1, there is effect of time on the results.

When comparing the analysis with irregularities and irregularities and spatial variability, it follows that a small distinction exists on both H_{max} and H_{rms} . For wavelengths between 4 and 6 the analysis considering spatial variability gives smaller values of H_{max} and H_{rms} , while for greater wavelengths the analysis with spatial variability gives greater values.

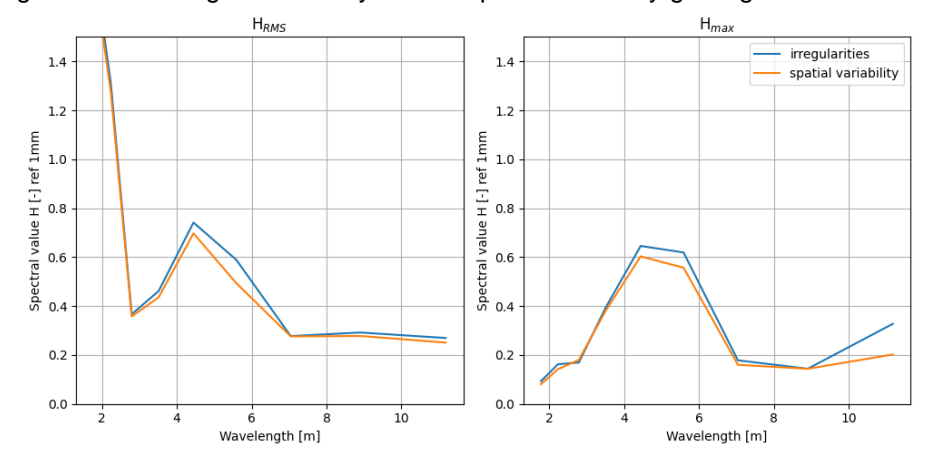


Figure 4.17 New parameter H_{max} and H_{rms} at a transition zone (stiff to soft subsoil).

4.3.2 Rail joint

4.3.2.1 Soft subsoil

Figure 4.18 shows the parameters H_{max} and H_{rms} for a rail joint on a soft subsoil. Again, there is no effect of time on the results. Comparing the effect of spatial variability, it follows that there are small differences between the two analyses (with and without spatial variability), for both parameters H_{max} and H_{rms} , for wavelengths between 4 and 8 m.

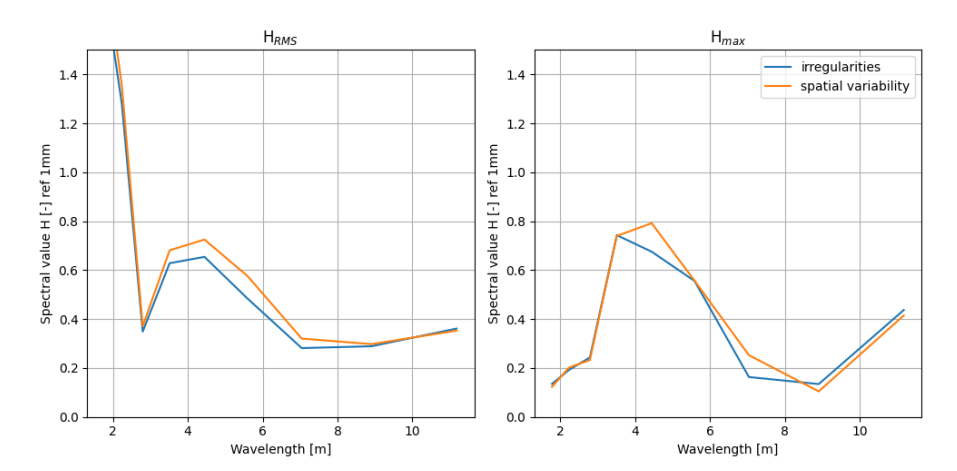


Figure 4.18: New parameter H_{max} and H_{rms} at a rail join (on soft subsoil).

4.3.2.2 Stiff subsoil

Figure 4.19 shows the parameters H_{max} and H_{rms} for a rail joint on a stiff subsoil. Similar to the previous analysis, there is no effect of time on the results. On a stiff subsoil the results show that the differences between the two analyses (with and without spatial variability) are neglectable.

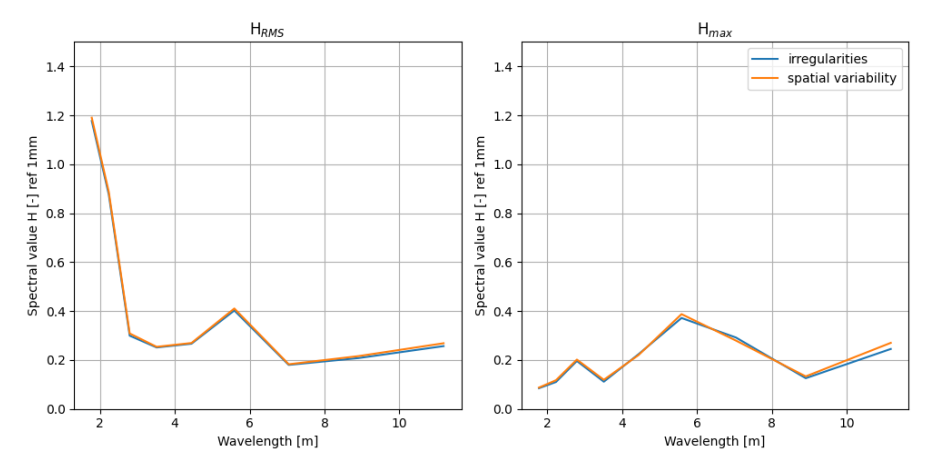


Figure 4.19 New parameter H_{max} and H_{ms} at a rail join (on stiff subsoil).

4.3.3 Discussion on parameters H_{max} and H_{RMS}

The two new parameters H_{max} and H_{rms} give little insight into variation of the cumulative railway track deformation in time. The analysis show that the H_{max} and H_{rms} parameters are constant at different moments in time (122, 243, 365 days – see Figure 4.15), while the railway track deformation varies significantly at these moments in time (see Figure 4.3 and Figure 4.4).

This is likely related to the fact the new parameters H_{max} and H_{rms} , are only defined for wavelengths between 1.6 and 11 m. The railway track deformation caused by the spatial variability, as modelled in this report, occurs at greater wavelengths. The railway track deformation caused by the rail irregularities and by the discontinuities occurs at lower wavelengths. Therefore, both these effects are not well captured by the H_{max} and H_{rms} parameters.

The analyses also show that there is little difference between the effect of rail irregularities and rail irregularities combined with the subsoil spatial variability on the H_{max} and H_{rms} parameters, while the railway track deformation is significantly different on both cases.

5 Conclusions and recommendations

This report summarises the work that has been performed to assess the influence of railway track degradation on the vibration generation. In the Introduction the following questions have been posed:

- 1. How does the "track vibration quality" develop over time at track objects (crossing structures and ES-joints) given a train loading scenario?
- 2. Does a reduction in maintenance intervals at track objects result in a proportionally higher track vibration quality?

In this report these questions have been addressed and answered.

5.1 Conclusions

Our findings concern the analysis of railway track deformation for two track objects: transition zone and rail joint. Both objects have been studied for two different subsoil schematisations: stiff and soft subsoil. The results of the railway track deformation have been used to compute the parameters H_{max} and H_{rms} , as suggested in [1]. These two parameters aim at establishing a relation between the track geometry and railway induced vibration.

The analyses on both objects show that spatial variability is more important than rail irregularities, when addressing railway track deformation. The model is able to distinguish between ballast compaction and subsoil creep and consolidation and it is shown that initially ballast compaction dominates the track deformation, but after a certain period of time subsoil creep and consolidation become dominant.

The results on the transition zone show that the displacement is greater close to the transition zone than on the free track further away from the transition zone, which is in agreement with experimental reports from literature (e.g. [35-36]). For the rail joint, it is found that its presence is not visible when considering rail irregularities and/or spatial variability of the subsoil. This is in agreement with the literature, which state that the presence of rail joints have an impact at high frequencies (> 500 Hz), which are not relevant for railway track deformation [9]. It must be noted that the effect of rail joint might be more pronounced if a gap is present. In the current modelling strategy this effect was not taken into account.

5.1.1 How does the "track vibration quality" develop over time at track objects (crossing structures and ES-joints) given a train loading scenario?

The results presented in this report show that the track vibration quality parameters H_{max} and H_{rms} , as suggested in [1] do not change with time. For a given object (transition zone or rail joint) the H_{max} and H_{rms} parameters are constant at different moments in time (122, 243, 365 days – see Figure 4.15), while the railway track deformation varies significantly at these moments in time (see Figure 4.3 and Figure 4.4).

It must be highlighted that this does not mean that railway track deformation does not have an influence on the railway induced vibrations, but rather that the effect of the railway track deformation is not captured by the parameters H_{max} and H_{rms} .

5.1.2 Does a reduction in maintenance intervals at track objects result in a proportionally higher track vibration quality?

Since the parameters H_{max} and H_{rms} do not change in time it is not possible to answer this question in a quantitative way. The fact that track geometry and geometry defects and variations affect railway induced vibrations is well established in literature (e.g. [37]).



However, in literature there is not yet a direct relation between the track geometry quality and the level of expected railway induced vibrations. Looking at the results presented in this report (e.g. Figure 4.4 and Figure 4.7) it is expected that keeping a better track geometry alignment by means of maintenance will lead to a reduction of the generation of railway induced vibrations. However, with the current model it is not possible to make a quantification of this improvement.

5.2 Recommendations

The parameters H_{max} and H_{rms} , aim at establishing the relationship between railway track deformation and railway induced vibration.

Based on the analysis it is advised to extend these parameters in order to account for the effects of spatial variability, railway irregularities and discontinuities. In particular, the parameters H_{max} and H_{rms} are only defined for wavelengths between 1.6 and 11 m. It would be beneficial to extend these parameters to lower and greater wavelengths, that can capture the above-mentioned effects. The results provided in this report can be used to test the new parameter definition.

The parameters H_{max} and H_{rms}, are based on the assumptions that the railway track geometry influences the induced vibrations, and that maintenance can reduce the magnitude of railway induced vibrations. These assumptions need to be further validated.

The relation of railway track deformation and railway induced vibrations can be studied by means of a more advanced model (e.g. STEM [38]). This could give additional information for the establishment of a relationship between the railway track deformation and railway induced vibrations. This would involve modelling the subsoil as a full three-dimensional volume and the quantification the wave propagation at several distances from the track. The results provided on this report can be used as an input for such analyses. Additionally, the experimental work that it is currently being performed in IBS can provide insights into the above-mentioned assumptions and provide guidance towards improvements of the parameters H_{max} and H_{rsm}. Should the quality parameters for railway track vibration prove successful in estimating induced vibrations, it could lead to the definition of threshold values for track quality based on desired levels of vibration quality.



6 References

- [1] A. Koopman, 'Trillingskwaliteit spoor', Level Accoustics & Vibration, LA.200902.R01, 2022.
- [2] A. Noordam and B. Zuada Coelho, 'ROSE'. Accessed: Feb. 13, 2023. [Online]. Available: https://github.com/PlatypusBytes/ROSE
- [3] J. N. Varandas, P. Hölscher, and M. A. G. Silva, 'Dynamic behaviour of railway tracks on transitions zones', *Computers & Structures*, vol. 89, no. 13–14, pp. 1468–1479, Jul. 2011, doi: 10.1016/j.compstruc.2011.02.013.
- [4] B. Zuada Coelho, J. N. Varandas, M. P. Hijma, and A. Zoeteman, 'Towards network assessment of permanent railway track deformation', *Transportation Geotechnics*, vol. 29, p. 100578, May 2021, doi: 10.1016/j.trgeo.2021.100578.
- [5] J. N. G. S. P. Timoshenko, *Theory of Elasticity*, 3rd edition. McGraw-Hill Education, 1970.
- [6] W. M. Zhai, 'Two simple fast integration methods for large-scale dynamic problems in engineering', International Journal for Numerical Methods in Engineering, vol. 39, pp. 4199–4214, 1996.
- [7] Q.-L. Zhang, A. Vrouwenvelder, and J. Wardenier, 'Numerical simulation of train-bridge interactive dynamics', *Computers & Structures*, vol. 79, no. 10, pp. 1059–1075, Apr. 2001, doi: 10.1016/S0045-7949(00)00181-4.
- [8] X. Lei and N.-A. Noda, 'ANALYSES OF DYNAMIC RESPONSE OF VEHICLE AND TRACK COUPLING SYSTEM WITH RANDOM IRREGULARITY OF TRACK VERTICAL PROFILE', Journal of Sound and Vibration, vol. 258, no. 1, pp. 147–165, Nov. 2002, doi: 10.1006/jsvi.2002.5107.
- [9] E. Kabo, J. C. O. Nielsen, and A. Ekberg, 'Prediction of dynamic train-track interaction and subsequent material deterioration in the presence of insulated rail joints', *Vehicle System Dynamics*, vol. 44, no. sup1, pp. 718–729, Jan. 2006, doi: 10.1080/00423110600885715.
- [10] J. P. Wolf and A. J. Deeks, 'Foundation vibration analysis: a strength-of-materials approach', *Choice Reviews Online*, vol. 42, no. 01, pp. 42-0328-42–0328, Sep. 2004, doi: 10.5860/CHOICE.42-0328.
- [11] R. Cairo, E. Conte, and G. Dente, 'Simplified Methods for the Dynamic Analysis of Single Pile in Layered Soils', 2001.
- [12] S.-H. Ju, H.-T. Lin, and J.-Y. Huang, 'Dominant frequencies of train-induced vibrations', *Journal of Sound and Vibration*, vol. 319, no. 1–2, pp. 247–259, Jan. 2009, doi: 10.1016/j.jsv.2008.05.029.
- [13] B. Zuada Coelho and M. A. Hicks, 'Numerical analysis of railway transition zones in soft soil', Proceedings of the Institution of Mechanical Engineers, Part F: Journal of Rail and Rapid Transit, vol. 230, no. 6, pp. 1601–1613, Aug. 2016, doi: 10.1177/0954409715605864.
- [14] W. Powrie, L. Le Pen, D. Milne, and D. Thompson, 'Train loading effects in railway geotechnical engineering: Ground response, analysis, measurement and interpretation', *Transportation Geotechnics*, vol. 21, p. 100261, Dec. 2019, doi: 10.1016/j.trgeo.2019.100261.



- [15] J. N. Varandas, P. Hölscher, and M. A. Silva, 'Settlement of ballasted track under traffic loading: Application to transition zones', *Proceedings of the Institution of Mechanical Engineers, Part F: Journal of Rail and Rapid Transit*, vol. 228, no. 3, pp. 242–259, Mar. 2014, doi: 10.1177/0954409712471610.
- [16] M. J. Shenton, 'Ballast deformation and track deterioration', in *Track technology*, Thomas Telford Publishing, 1985. doi: 10.1680/tt.02289.
- [17] Y. Sato, 'Japanese Studies on Deterioration of Ballasted Track', Vehicle System Dynamics, vol. 24, no. sup1, pp. 197–208, Jan. 1995, doi: 10.1080/00423119508969625.
- [18] R. Ford, 'Differential Ballast Settlement, and Consequent Undulations in Track, Caused by Vehicle-Track Interaction', Vehicle System Dynamics, vol. 24, no. sup1, pp. 222–233, Jan. 1995, doi: 10.1080/00423119508969627.
- [19] E. T. Selig and J. M. Waters, *Track geotechnology and substructure management*. London: New York: T. Telford; American Society of Civil Engineers, Publications Sales Dept. [distributor], 1994.
- [20] T. Dahlberg, 'Some railroad settlement models—A critical review', Proceedings of the Institution of Mechanical Engineers, Part F: Journal of Rail and Rapid Transit, vol. 215, no. 4, pp. 289–300, Jul. 2001, doi: 10.1243/0954409011531585.
- [21] T. D. Stark, S. T. Wilk, J. R. Rose, and W. Moorhead, 'Effect of hand tamping on transition zone behavior', in *Proc: 2015 American Railway Engineering and Maintenance-of-Way Association Conference*, 2015.
- [22] B. Zuada Coelho, J. Priest, and P. Hölscher, 'Dynamic behaviour of transition zones in soft soils during regular train traffic', *Proceedings of the Institution of Mechanical Engineers, Part F: Journal of Rail and Rapid Transit*, vol. 232, no. 3, pp. 645–662, Mar. 2018, doi: 10.1177/0954409716683078.
- [23] L. Mauer, 'An Interactive Track-Train Dynamic Model for Calculation of Track Error Growth', *Vehicle System Dynamics*, vol. 24, no. sup1, pp. 209–221, Jan. 1995, doi: 10.1080/00423119508969626.
- [24] D. Li and E. T. Selig, 'Cumulative Plastic Deformation for Fine-Grained Subgrade Soils', *Journal of Geotechnical Engineering*, vol. 122, no. 12, pp. 1006–1013, Dec. 1996, doi: 10.1061/(ASCE)0733-9410(1996)122:12(1006).
- [25] C. Charoenwong, D. P. Connolly, P. K. Woodward, P. Galvín, and P. Alves Costa, 'Analytical forecasting of long-term railway track settlement', *Computers and Geotechnics*, vol. 143, p. 104601, Mar. 2022, doi: 10.1016/j.compgeo.2021.104601.
- [26] S. Müller, L. Schüler, A. Zech, and F. Heße, 'GSTools v1.3: a toolbox for geostatistical modelling in Python', *Geosci. Model Dev.*, vol. 15, no. 7, pp. 3161–3182, Apr. 2022, doi: 10.5194/gmd-15-3161-2022.
- [27] R. H. Kraichnan, 'Diffusion by a Random Velocity Field', *Phys. Fluids*, vol. 13, no. 1, p. 22, 1970, doi: 10.1063/1.1692799.
- [28] F. Heße, V. Prykhodko, S. Schlüter, and S. Attinger, 'Generating random fields with a truncated power-law variogram: A comparison of several numerical methods', *Environmental Modelling & Software*, vol. 55, pp. 32–48, May 2014, doi: 10.1016/j.envsoft.2014.01.013.
- [29] K.-K. Phoon and F. H. Kulhawy, 'Characterization of geotechnical variability', vol. 36, p. 13, 1999.



- [30] X. Nie, J. Zhang, H. Huang, Z. Liu, and S. Lacasse, 'Scale of Fluctuation for Geotechnical Probabilistic Analysis', presented at the Geotechnical Safety and Risk V, 2015, pp. 834–840. doi: doi:10.3233/978-1-61499-580-7-834.
- [31] H. Wang and V. L. Markine, 'Methodology for the comprehensive analysis of railway transition zones', *Computers and Geotechnics*, vol. 99, pp. 64–79, Jul. 2018, doi: 10.1016/j.compgeo.2018.03.001.
- [32] C. Esveld, Modern railway track, vol. 385. MRT-productions Zaltbommel, 2001.
- [33] SPC00342-1, 'Prefab gelijmde ES-lassen voor 54E1 en 60E1 spoorstaafprofiel', SPC00342-1, 2022.
- [34] T. D. Stark, S. T. Wilk, H. B. Thompson, T. R. Sussmann, M. Baker, and C. L. Ho, 'Evaluating Fouled Ballast Using Seismic Surface Waves', in 2016 Joint Rail Conference, Columbia, South Carolina, USA: American Society of Mechanical Engineers, Apr. 2016, p. V001T01A002. doi: 10.1115/JRC2016-5714.
- [35] D. Li, 'Deformations and Remedies for Soft Railroad Subgrades Subjected to Heavy Axle Loads', in Advances in Transportation and Geoenvironmental Systems Using Geosynthetics, Denver, Colorado, United States: American Society of Civil Engineers, Jul. 2000, pp. 307–321. doi: 10.1061/40515(291)20.
- [36] D. Li, D. Otter, and G. Carr, 'Railway Bridge Approaches under Heavy Axle Load Traffic: Problems, Causes, and Remedies', *Proceedings of the Institution of Mechanical Engineers, Part F: Journal of Rail and Rapid Transit*, vol. 224, no. 5, pp. 383–390, Sep. 2010, doi: 10.1243/09544097JRRT345.
- [37] G. Kouroussis, D. P. Connolly, G. Alexandrou, and K. Vogiatzis, 'The effect of railway local irregularities on ground vibration', *Transportation Research Part D: Transport and Environment*, vol. 39, pp. 17–30, Aug. 2015, doi: 10.1016/j.trd.2015.06.001.
- [38] STEM, 'STEM'. StemVibrations, Sep. 14, 2023. Accessed: Oct. 06, 2023. [Online]. Available: https://github.com/StemVibrations/STEM



Appendix A

Table A.1 Lithological description and geomechanical soil parameterisation for the soil layers.

Soil lithology	Description	Geological formation	Unit weight [kN/m³]	Dynamic Young modulus [MPa]	Poisson ratio [-]	Damping ratio [%]
H_Aa_ht	Anthropogenic soil layer, mixture of sand and clay	None	20	30	0.4	2
H_Vbv_v	Basal peat, compact thin layer	Nieuwkoop	11	5	0.45	2
H_Vhv_v	Peat, soft	Nieuwkoop	10	5	0.45	2
H_Rk_k&v	Lower flood-basin deposit, clay and peat	Echteld	15.5	78	0.45	2
H_Rk_vk	Lower flood-basin deposit, clayey peat	Echteld	14	62	0.45	2
H_Rk_k	Higher flood-basin deposits, clay and silty clay	Echteld	15.5	62	0.45	2
H_Ro_z&k	Natural-levee deposits, silty/sandy clay and sand	Echteld	17.5	107	0.4	2
H_Rr_o&z	Residual-channel deposit, both organic and sandy layers	Echteld	16	80	0.4	2
H_Rg_zm	Channel-bed deposit, fine to very coarse sand	Echteld	20	472	0.4	2
P_Wrd_zm	Aeolian deposit (Pleistocene): fine to medium sand	Kreftenheye (Delwijnen member)	20	191	0.4	2
P_Rk_k&s	Flood-plan/basin deposit (Pleistocene): loam	Kreftenheye (Wijchen Member)	19.5	92	0.45	2
P_Rg_zm	Channel-bed deposit (Pleistocene): medium to coarse sand	Kreftenheye, Beegden, Sterksel	20	191	0.4	2

Deltares is an independent institute for applied research in the field of water and subsurface. Throughout the world, we work on smart solutions for people, environment and society.

Deltares